Available online at www.sciencedirect.com
ScienceDirect
Acta Materialia 57 (2009) 2800–2811
Acta MATERIALIA
www.elsevier.com/locate/actamat

Effect of fatigue on the interface integrity of unidirectional C_f-reinforced epoxy resin composites

Christos Koimtzoglou [a,c], Konstantinos G. Dassios [b], Costas Galiotis [a,b,*]

[a] *Foundation for Research and Technology Hellas, Institute of Chemical Engineering and High Temperature Processes, Stadiou Street, Platani, Patras GR-26504, Greece*
[b] *Department of Materials Science, University of Patras, Rio GR-26504, Greece*
[c] *Integrated Aerospace Sciences Corporation, 17 Tegeas Street, Argyroupolis, Athens, GR-16452, Greece*

Received 1 October 2008; received in revised form 23 February 2009; accepted 24 February 2009
Available online 1 April 2009

Abstract

The current study reports on the fatigue behaviour, micromechanics of reinforcement and stress transfer efficiency of the interface of an autoclave-processed C_f-epoxy laminate. Throughout fatigue loading at a maximum strain below the critical fatigue limit of the matrix material, testing was interrupted at discrete fatigue levels of 10^0, 10^3, 10^4 and 10^5 cycles to allow for laser Raman microscopy measurements of the axial stresses developing along natural and induced discontinuities on fibres in the composite. The established axial stress profiles were regressed to establish the corresponding interfacial shear stress (ISS) profiles at each fatigue level. The effect of fatigue on the stress transfer efficiency of the interface was calculated through the evolution of three interfacial performance parameters (maximum ISS, length required for its attainment and transfer length) as a function of loading cycles. Additional measurements on "random" locations helped identify the main damage mechanisms developing at the microscale.

Keywords: Composite; Carbon fibre; Raman spectroscopy; Fatigue; Interface

1. Introduction

Owing mainly to their high strength-to-weight ratio but also to their stress redistribution capacity, polymer matrix composites have been emerging as a favourable candidate material for aeronautical and structural application over the last 20 years. While their fracture processes under static or impact conditions have been extensively investigated in the past, the fatigue behaviour has been given much less research attention. This fact is mainly due to the complexity associated with comprehending the role and dynamics of the interactions of each of the constituents of the composite, namely the matrix, reinforcing fibres and the interface under fatigue. This complexity comes, in turn, as a result of the difficulty in recording the stress state in these constituents at the microscale, especially under time-variable loading conditions. There is also the general feeling that polymer matrix composites behave well under fatigue loading. However, this cannot be true for any fibre/matrix combination or geometrical configuration.

There seems to be very little information in the literature concerning the effect of fatigue loading on the integrity of the interface prior to catastrophic failure of the composite. It has, however, been shown that the interface friction plays an important role in resisting debonding by crack growth, but the degradation of interface friction due to cyclic loading can reduce the friction stress [1]. Furthermore, the interfacial shear stresses (ISS) seem to be insensitive to the increase of loading frequency in pristine materials, while the presence of stress-induced matrix and fibre cracks can lead to pronounced changes of ISS with frequency [2].

---

[*] Corresponding author. Address: Foundation for Research and Technology Hellas, Institute of Chemical Engineering and High Temperature Processes, Stadiou Street, Platani, Patras GR-26504, Greece.
E-mail address: c.galiotis@iceht.forth.gr (C. Galiotis).

1359-6454/$36.00 © 2009 Acta Materialia Inc. Published by Elsevier Ltd. All rights reserved.
doi:10.1016/j.actamat.2009.02.038

The deleterious effect of compressive loads in the loading cycle of multidirectional composites is attributed to the more rapid debond growth around the transverse fibres in T–C loading [3]. In composites with short fibres, it has been shown that a radial tensile stress is generated at the interface as a result of fatigue loading, which can be higher than the interfacial shear stress in matrices showing elastoplastic behaviour and can induce fibre/matrix debonding [4]. The above very limited information on the effect of fatigue on interfacial integrity indicates the necessity of additional research on the specific area that would ideally capture the change in interfacial parameters directly at the microscale.

To date, laser Raman microscopy (LRM) is the only experimental technique able to measure stress or strain on individual fibres at the microscopic level. The principles governing the technique have been presented in previous publications [5]. In short, the Raman wavenumbers of certain vibrational modes of crystalline materials – such as carbon and Kevlar fibres embedded in composites – are stress/strain dependent, most frequently through a simple linear relation that can be established experimentally. This relation between stress/strain and Raman shift constitutes the fibre-specific Raman calibration curve which can be used reversely to translate shifts captured from the same type of fibre in a composite material, to stress/strain. It is important to note that, as an optical technique, LRM can only capture strain or stress on fibres that are visible at the outer surface of the composite. Thus, an epoxy matrix system offering a certain degree of transparency is desirable as it makes possible the collection of spectra from fibres embedded just below the composite's surface. Stress distributions along individual embedded fibres can then be established through the collection of consecutive spectra along the fibre length and can be converted into interfacial shear stress (ISS) profiles by means of a straightforward balance of shear-to-axial forces argument [5]. This argument leads to a simple analytical expression between the ISS, τ_{rx}, acting at the surface of the fibre and the gradient of the stress transfer profiles:

$$\tau_{rx} = -\frac{r}{2}\frac{\mathrm{d}\sigma_f}{\mathrm{d}x} \qquad (1)$$

where σ_f is the fibre axial stress, r is the radius of the fibre and x is the distance along the length of the fibre. Hence, the LRM technique can not only measure the stress/strain state of individual reinforcing fibres in the microscale but also provide information on the ISS distribution, and therefore the stress transfer efficiency of the system.

The LRM technique was successfully employed in a previous pilot study [6] to measure the ISS, the transfer length for efficient stress built-up and the length required for the attainment of maximum ISS in model single-carbon-fibre composite geometries loaded in tension–tension fatigue. In the present work, the LRM methodology is used to quantify the micromechanics of tension–tension fatigue loading of unidirectional M40 C_f-epoxy laminates embodying the same constituents (matrix, fibres) as the model composites. Coupon geometries of the composite material are subjected to cyclic loads at a maximum strain below the critical fatigue limit of the matrix material, and the LRM probe is used to capture the initiation and evolution of damage in the fibres and the fibre–resin interface directly at the microscale and in real time.

2. Experimental

2.1. Laser Raman microscopy

A compact remote LRM system, "ReRaM 3" (remote Raman microscope), equipped with polarization-preserving fibre optics for transferring the signal to a distant spectrometer (Model 1000 M Single Monochromator, SPEX, SPEX Industries Inc., Edison, NJ) was used for the collection of spectra on loaded fibres within the composite. The integrated miniature diode-pumped solid-state laser source of the Raman microscope (custom-built by Dilor/Jobin Yvon SAS, Lille, France) transmitted a monochromatic radiation of a wavelength of 532 nm at a power of 50 mW. The power of the incident radiation could be adjusted between 0.5 and 13.8 mW by means of various density filters. Different objective lenses were used to adjust the microscope's magnification power between ×4 and ×80, thus allowing both macroscopical observations of the damage as well as high resolution spectroscopic measurements. The whole system rested in front of a servo-hydraulic testing frame (Model 858 Tabletop, MTS Systems Corp., Eden Prairie, MN) and was mounted on a micro-translational stage able to travel the microscope in discrete steps of 1.2 μm in three dimensions to facilitate focusing of the laser beam on distinct fibres during mechanical testing. The spectroscopic signal was transferred from the remote microscope to the spectrometer with the aim of a fibre optic cable where it was analyzed in terms of Raman wavenumber shifts. The polarization of the excitation radiation was set parallel to the fibres' orientation, which is also parallel to the loading direction. The peak used in the current study to convert the Raman shifts (captured from M40 fibres at the surface of the laminate) to strain/stress is the E_{2g} graphite vibrational mode (at $1580\ \mathrm{cm}^{-1}$ Raman wavenumbers) with a stress sensitivity of $-3.0\ \mathrm{cm}^{-1}\ \mathrm{GPa}^{-1}$ [6].

2.2. Materials and specimens

The composite materials used in this project were unidirectional carbon-fibre-reinforced epoxy matrix laminates processed from prepreg sheets under vacuum-assisted thermal curing in a semi-industrial autoclave furnace (Aeroform Industrial Controls Ltd, UK). The carbon fibres were high modulus grade M40-40B (Toray, Japan) while the matrix was high viscosity EF2600 epoxy resin (Shell Chemicals). Rectangular specimens of dimensions of 230 mm length, 12.7 mm width and 1 mm thickness

(ASTM D 3039/D 3039M-95a and ASTM D 3479/D 3479M-96) were cut from the resulting 230 mm × 300 mm plate.

2.3. Testing

Mechanical testing under tensile and fatigue conditions was performed with simultaneous LRM measurements of stress on distinct fibres at the microscale. The tests were performed on a MTS® 858 Mini Bionix hydraulic frame under crosshead displacement control with a rate of 1 mm min^{-1} (ASTM D 3039/D 3039M-95a). Strain was measured using strain gauges of a gauge factor of $f_g = 2.1$ (Kyowa KFG-5-120-C1-11L1M2R). Due to the acquisition times associated with the acquisition of spectra, the loading procedure had to be interrupted in frequent intervals, under displacement-hold condition, in order to allow for LRM scanning of the fibres with the Raman microprobe.

2.3.1. Tensile loading with simultaneous Raman measurements

Static tensile loading with parallel LRM measurements was performed on eight M40-40B/epoxy specimens. The loading procedure was interrupted in consecutive deformation levels for 24 h to allow the acquisition of multiple spectra at different positions along the fibres. It is important to note that, during interruptions, the specimen was held at constant strain. The timescale and loading flow of the experiments is shown in Fig. 1 where the interruptions for LRM measurements are represented as constant-strain steps.

The Raman measurements during constant stress were performed along either side of discontinuities on carbon fibres that were visible on the outer surface on the specimens. The scanned length was 750 μm on either side of the discontinuity, while the step of LRM acquisitions was 2.5 μm close to the discontinuity in order to capture as closely as possible the whole build-up of the axial stresses on the fibres. This step was increased gradually to 25 μm at the far end of the scanned length.

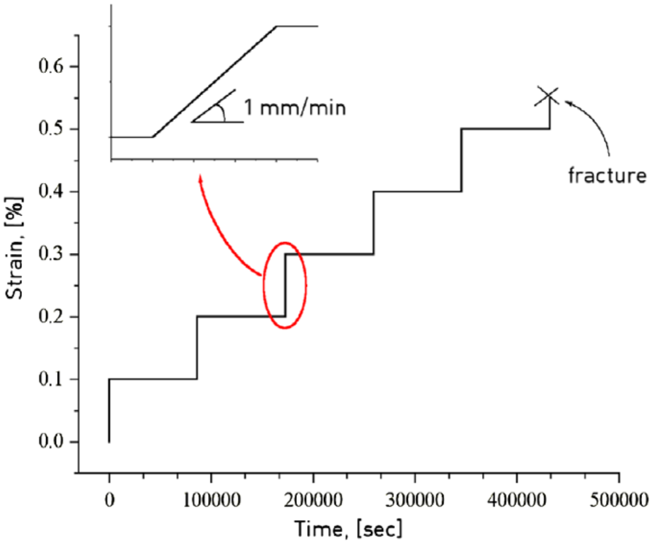

Fig. 1. Loading procedure of the tensile tests with parallel Raman measurements.

Since fibre failures could not appear at low levels of externally applied deformation, pre-existing fibre "failures" were introduced into a number of specimens just before the curing procedure. These discontinuities were generated with the careful use of surgical scalpel under optical microscope magnification following a previously developed technique [7]. These discontinuities were induced at certain locations of the outer laminas of the composite plate while their size (length and depth) was chosen to be as small as possible in order not to affect the mechanical properties of the composite material. The procedure for the creation of induced discontinuities in the carbon fibres is shown in Fig. 2.

2.3.2. Fatigue loading with simultaneous Raman measurements

Two specimens were subjected to fatigue loading with parallel Raman measurements. The imposed loading waveform was sinusoidal with a frequency of 10 Hz and a loading ratio (minimum/maximum applied load) of $R = 0.1$ according to ASTM D 3479/D 3479M-96. The maximum applied load was 80% and 90% of the static strength of the composite material. Raman measurements were performed after the first (static) loading, as well as after 10^3, 10^4, 10^5, 5×10^5 end 10^6 loading cycles. To conduct the Raman measurements at each of these steps, the cyclic loading was interrupted for approximately 48 h. It was decided that, during interruption of the cyclic loading procedure, the deformation of the specimen should remain constant, at the value corresponding to the maximum applied force of the cycle. Fig. 3 depicts the loading protocol followed in the interrupted fatigue testing.

Using the same methodology as in the tensile tests, Raman measurements were conducted on fibre discontinuities, either fibre failure locations or induced fibre ends, visible at the outer surface of the loaded specimen. Additionally, 200 measurements during each interruption were performed at "random" locations (irrespective of discontinuity locations) defined as the knots of an imaginable 20 × 10 matrix grid around the centre of the specimen (Fig. 4). The step size along the grid longer dimension, which was parallel to the specimen loading axis, was 400 μm, while a step of 700 μm was used for the measurements across the specimen's width. The step sizes were chosen to be safely greater than both inter-fibre separation and the stress transfer length, L_t of the specific composite material system, so that it is impossible for any pair of measurements to correspond to the same axial stress build-up [8,9].

3. Results

3.1. Tensile loading with simultaneous Raman measurements

One of the biggest problems encountered during the LRM measurements was the detection of fibre discontinu-

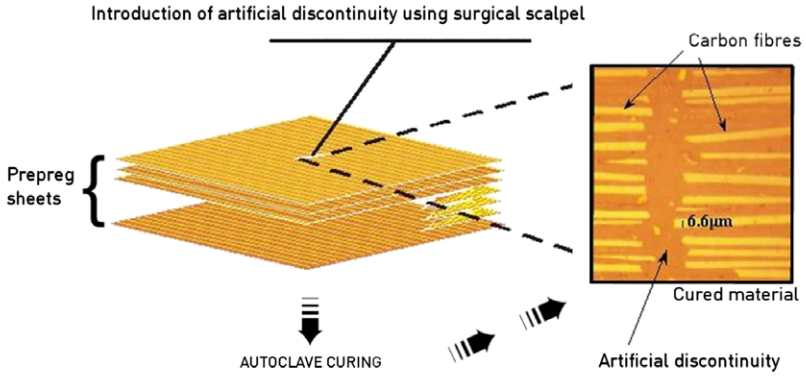

Fig. 2. Introduction of induced discontinuities on carbon fibres at the surface of composite plates. On the right is an optical microscope photograph of the discontinuity on the surface of the cured composite.

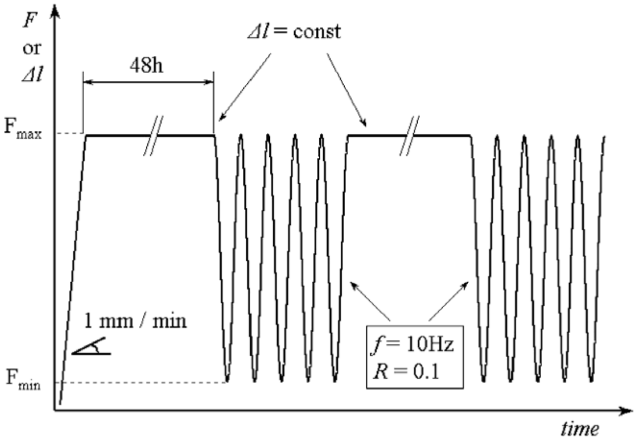

Fig. 3. Loading protocol of the interrupted fatigue tests with parallel Raman measurements.

ity/failure locations, especially at low applied strains. This issue was effectively confronted by the introduction of induced discontinuities prior to autoclave curing of the laminate, as explained above. A second experimental difficulty was finding, at the surface of the material, fibres (with discontinuity) of sufficient length to allow capturing the whole axial stress build-up effect alongside the discontinuity. It is known that during prepreg production, fibres do not remain completely parallel with each other but can weave or change plane at random locations. As a result, very frequently a continuous fibre at the outer surface of the specimen with a visible discontinuity can hide below other fibres close enough to the discontinuity and thus prevent measurements of the load build-up. In the following analysis, the axial and interfacial shear stress profiles and interfacial parameters are presented indicatively for one specimen, while the findings did not vary significantly among specimens. The profiles presented here were obtained by selecting fibres that were free of the problems described above.

The axial stress distributions captured via the Raman probe alongside an induced fibre discontinuity on specimen “itns-07” are presented in Figs. 5–7 for consecutive levels of externally applied strain. The experimental data are represented by open cycle symbols while the cubic spline regression is shown as a solid line through the data. In

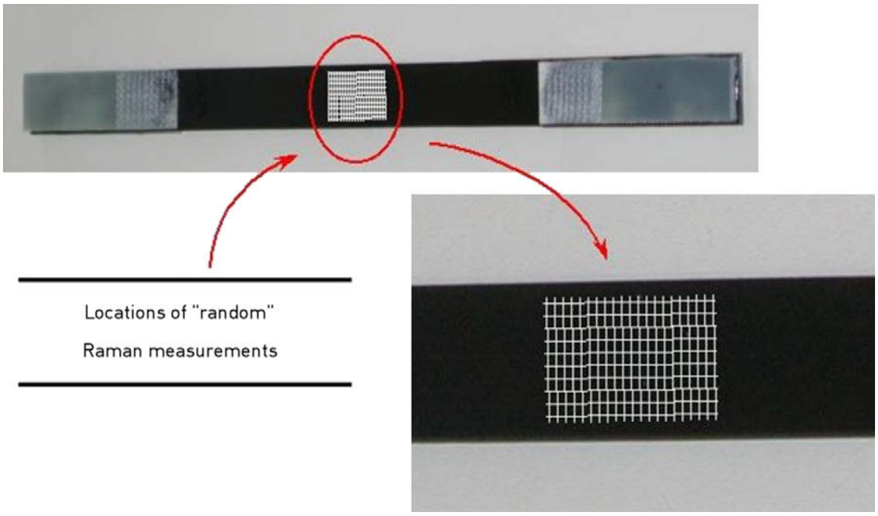

Fig. 4. Picture of a M40-40B/epoxy specimen and the position of the grid used for the “random” Raman measurements.

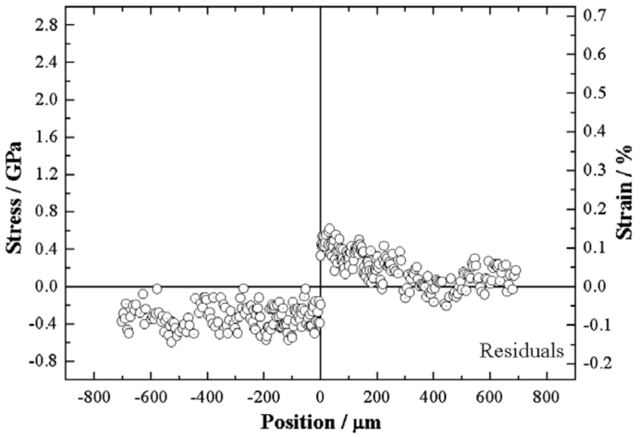

Fig. 5. Axial stress distribution alongside an induced fibre discontinuity at zero externally applied strain for specimen “itns-07”.

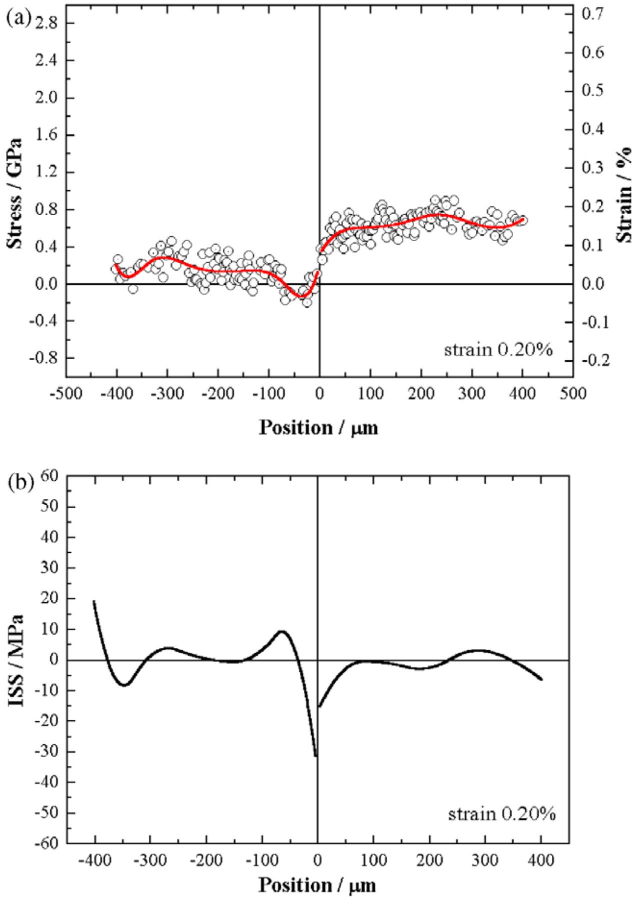

Fig. 6. Distribution of axial stresses (a) and of calculated interfacial shear stresses (b) on fibres alongside an induced discontinuity at 0.20% externally applied strain (specimen “itns-07”).

Fig. 7, graphs in column “b” present the stress distributions captured, at the same strain level, alongside a natural discontinuity that was found on the specimen surface. Each of the graphs in Figs. 5–7 carries a label indicating the level of externally applied strain when the distribution was captured as well as an equivalent strain axis on the right-hand side, calculated based on the fibres’ nominal elastic modulus (420 GPa, Toray Carbon Fibers America, Inc.). The ISS profiles were calculated by application of Eq. (1) to the regressions on the axial stress distributions. A representative ISS profile is shown in Fig. 6b for a strain level of 0.20%.

The distribution of axial stresses alongside an induced discontinuity after the autoclave curing procedure and at zero externally applied strain (stress-free state) is shown in Fig. 5. A clear difference is evident in the profiles on either side of the discontinuity, which indicates a possible effect of the cutting of the fibres using the surgical scalpel on the stress build-up scenario. Thereby, while one fibre end is under residual compressive stress of approximately −0.4 GPa (ca. −0.1% strain), the stress at the opposite fibre is tensile to 0.4 GPa (ca. 0.1% strain) at the fibre end and relaxes at a distance of 400 µm.

At the level of 0.2% externally applied strain (Fig. 6), axial stresses on the left fibre appear to start from zero at the fibre end, drop to marginally compressive values and attain a steady-state value of 0.2 GPa at approximately 150 µm from the discontinuity. Stress on the fibre to the right of the discontinuity is at the same value as in the stress-free case (0.4 GPa) at the fibre end, and rises to 0.6 GPa (0.15%) at a distance of 100 µm.

Further into loading, for externally applied deformations of 0.3–0.5% (Fig. 7), the axial stress distributions near both fibre ends appear to commence from the same values as in the previous case of 0.20% externally applied strain. The fully developed values of the profiles, at a distance of approximately 400 µm from each fibre end, increase with the level of externally applied strain in each step, with the value at the left fibre end resting consistently lower than that at the right end. It is also observed that the length required for the full development of the stresses, increases gradually from 100 µm at 0.3% applied strain to 250 and 300 µm at 0.4% and 0.5% applied strain, respectively.

In the case of the natural discontinuity (fibre failure), it is observed that the axial stress distributions start from approximately 0.5 GPa at the left fibre end and from 0.4 GPa at the right end at a strain level of 0.4% and decrease to 0.3 and 0.2 GPa, respectively, at the 0.5% applied strain level. These fibre-end values originate from the fibre recoiling effect acting immediately after fibre failure and the resulting relaxation (freezing) of the fibre ends at the stress level permitted by the radial and hoop stresses imposed to the interface by the matrix material [10]. The fully developed axial stress value for the fibre on the left of the natural discontinuity starts at 1.4 GPa (ca. 0.3% strain) at the 0.4% strain level and increases to 1.6 GPa (ca. 0.4% strain) at the 0.5% strain level. The corresponding length required for the attainment of the fully developed axial stress value is ca. 100 µm, irrespective of externally applied strain (Fig. 7b). In contrast, the shape of the axial stress profile of the fibre to the right of the natural discontinuity appears to have been influenced by the failure of a separate neighbouring fibre; hence a rise in axial stress is noted in distances larger than 250 µm from the discontinu-

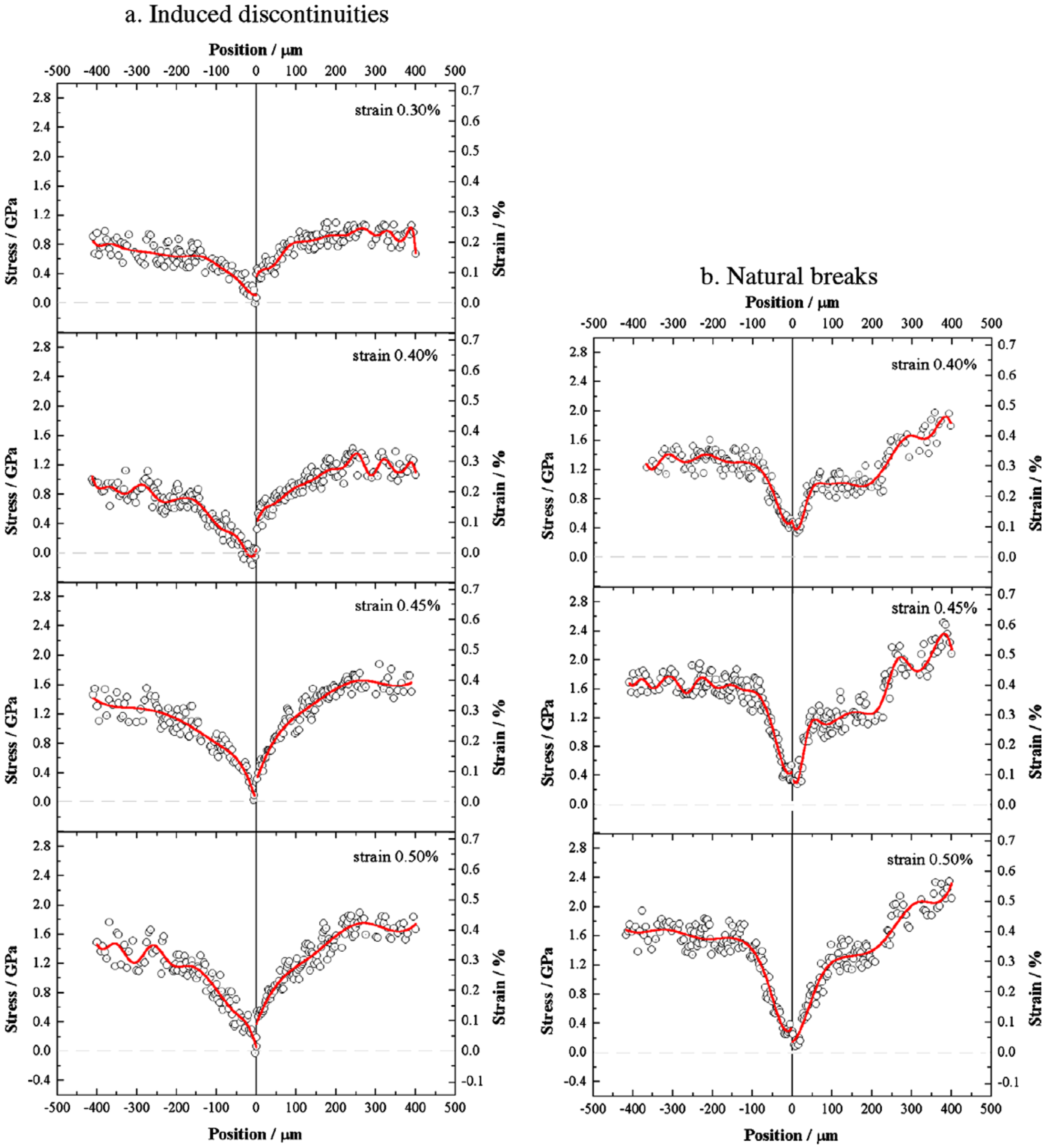

Fig. 7. Distribution of axial stresses on fibres alongside an induced (a) and a natural discontinuity (b) at 0.30%, 0.40%, 0.45% and 0.50% externally applied strain (specimen "itns-07").

ity which corresponds to the length at which the fully developed value is attained (Fig. 7). It should be noted that the location of such a neighbouring failure was sought with the microscope, nonetheless without success probably due to the fact that it rested in a lower plane beneath the interrogated fibre and it was inaccessible for optical observation.

The results of the cubic spline regressions to the axial stress profiles were introduced into Eq. (1) to obtain the ISS profiles. The main parameters that determine the stress transfer mechanism, hence the performance of the interface are: (i) the maximum value of the interfacial shear stress, ISS_{max}, (ii) the distance from the discontinuity required for the attainment of ISS_{max}, b, and (iii) the distance from ISS_{max} required for the relaxation of the ISS, L_t. Non-zero values of length b are indicative of the existence of interfacial failure. L_t is the stress transfer length, essentially the length required for the full build-up of the axial stresses or, in other words, the distance from the fibre end over which stresses are transferred from the matrix to the reinforcing fibres and beyond which the axial stresses on the fibre have attained their maximum values [11].

The ISS_{max}, b, and L_t were measured for the profiles established at each step of externally applied strain and their mean values from both sides of the discontinuity are presented in Fig. 8 along with graphical definitions of the three interfacial performance parameters. For the induced discontinuity, the mean value of ISS_{max} increases from 13 MPa at 0.2% applied strain to 28 MPa at 0.5% applied strain. In the case of the natural discontinuity, the same parameter takes values of 31, 42 and 28 MPa at 0.40%, 0.45% and 0.50% applied strain, respectively. The length b associated with the induced discontinuity is slightly greater than 30 µm at the first strain level and decreases to 0 µm at 0.45% applied strain. On the other hand, the same parameter in the case of the natural discontinuity remains constant at 40 µm throughout testing. Finally, the transfer length of the induced discontinuity increases from 100 to 230 µm throughout testing. The transfer length of the natural discontinuity starts at 100 µm and rises to 140 µm at the final step of externally applied strain.

The findings presented up to the current point for specimen “itns-07” are representative of the behaviour of all specimens tested in tension with simultaneous Raman measurements. For example, following the autoclave curing procedure of the material, residual stresses at fibre ends of induced discontinuities were found at compressive levels of approximately −0.4 GPa (ca. −0.1% strain) while tensile stresses recorded at certain fibre ends as side-effects of the discontinuity introduction technique remained in the vicinity of 0.4 GPa, commonly to the case of specimen “itns-07”. The axial stress build-up scenario and the stresses corresponding to the fully developed profiles also remained unchanged among different specimens and were in every case slightly lower that the externally applied strain. Differences in the axial stress build-up scenarios alongside natural and induced discontinuities were observed in each of the specimens tested, while all naturally induced fibre failures

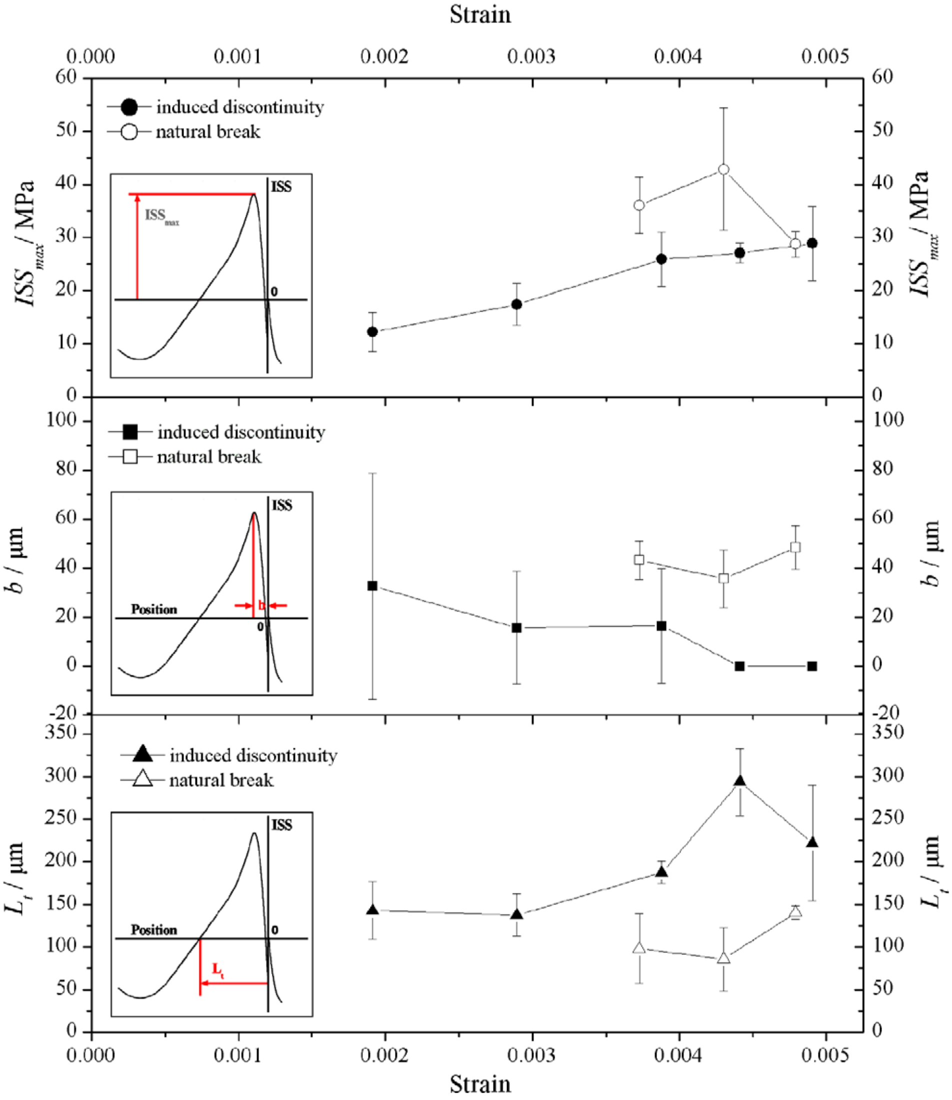

Fig. 8. Mean value of both fibre ends, of the maximum interfacial shear stress, ISS_{max}, of the distance b required for the attainment of ISS_{max}, and of the stress transfer length L_t, for each step of externally applied strain (specimen “itns-07”). Also shown in subset graphs are the graphical definitions of each parameter.

did not appear before 0.40% externally applied strain. Thus, the fully developed stresses around natural discontinuities were marginally higher and were attained in shorter distances that the corresponding values in the profiles of induced discontinuities. Additionally, stress build-up at the fibre ends commenced at different stress values between induced and natural discontinuities due to fibre recoiling effects in the latter case. The same phenomenon is responsible for the difference in stress at the two fibre ends, left and right, in the vicinity of the natural discontinuity. The interface performance parameters (ISS_{max}, b, L_t) established for specimen "itns-07" were indicative of the total of the specimens tested. For example, the maximum interfacial shear stress, ISS_{max}, is lower in the case of induced discontinuities than that of natural discontinuities. The same applies for the distance b from the fibre end over which the ISS_{max} is attained, a direct indicator of interfacial failure. The transfer length, L_t, was also found larger in stress distributions of induced discontinuities than the corresponding value associated with natural discontinuities.

3.2. Fatigue loading with simultaneous Raman measurements

3.2.1. Stress take-up from fibre discontinuities

Fatigue loading with simultaneous Raman measurements was performed on two specimens, "iftg-01" and "iftg-02". In common with tensile testing, the necessary condition for making successful measurements was the presence, on the surface of the specimen, of failed fibres that provide sufficient lengths alongside the discontinuity for capturing the stress build-up. This condition was fully met in specimen "iftg-01", while LRM measurements on specimen "iftg-02" were concentrated on an individual fibre end located at the surface of the specimen.

The axial stresses developing alongside the natural discontinuity on specimen "iftg-01", loaded at $0.90\sigma_{\mathrm{ult}}$ (90% of the static strength of the material), after 1 cycle are presented in Fig. 9. The equivalent strain axis on the right-hand side of Fig. 9a, is calculated based on the fibres' nominal elastic modulus. The specific specimen endured 4168 loading cycles, hence allowed the collection of only two sets of LRM data. In the same figures, the cubic spline regressions to the LRM stress data (open cycle symbols) are shown as solid lines, while graphs of column "b" represent the ISS profiles obtained through Eq. (1). The data in Fig. 9 demonstrate that, after the first loading cycle, and while the specimen is held at the strain level corresponding to the maximum stress of the fatigue cycle, the axial stresses on the fibres in the vicinity of the discontinuity are compressive to −0.25 GPa and attain a tensile fully developed value at a distance of 120 μm from the fibre end. The fully developed values differ between the two fibres, the left being at 1.7 GPa, while the right fibre stress was 2.1 GPa; a behaviour attributed to probable failures of neighbouring, out-of-plane fibres, as discussed in the previous section. The shapes of both axial and ISS profiles appear to remain practically unchanged after 10^3 loading cycles.

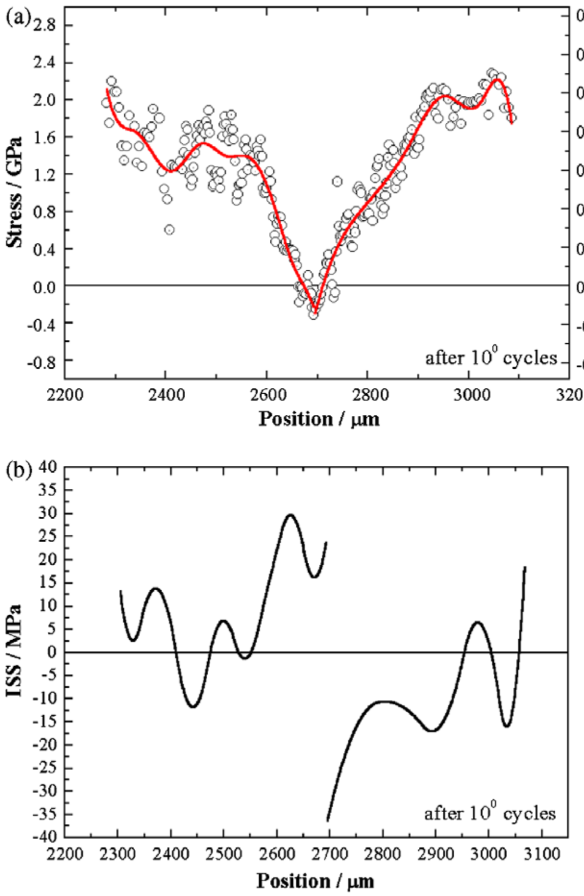

Fig. 9. Axial stress (a) and the obtained interfacial shear stress (b) profiles alongside a natural discontinuity after the first loading cycle (specimen "iftg-01").

The main parameters that characterize the stress transfer efficiency of the interface, ISS_{max}, b, L_t, are presented in Fig. 10 and indicate the negative influence of the cyclic loading on the performance of the interface. The maximum interfacial shear stress value of 26 MPa after 10^3 cycles has decreased by 7 MPa as compared to the first loading cycle. The length required for the attainment of the ISS_{max}, b, increases from 34 μm after the first cycle, to 49 μm after 10^3 cycles. The stress transfer length, L_t, appears not to be significantly affected by the cyclic loading procedure as it decreases only by 3 μm within the same range.

The effect of fatigue on the stress transfer mechanism is similar for specimen "iftg-02", loaded at $0.80\sigma_{ult}$. The specific specimen endured 136,264 loading cycles, hence allowed the collection of additional sets of LRM data. The measured axial stress profiles, and their cubic spline regressions after 1, 10^3, 10^4 and 10^5 loading cycles, are presented in Fig. 11. The graphs in this figure carry a label indicating the number of cycles the specimen had undergone before the profile was captured as well as an equivalent strain axis on the right-hand side, calculated based on the fibres' nominal elastic modulus.

After the first loading cycle, axial stresses start to build from 0.2 GPa at the fibre end and reach a fully developed

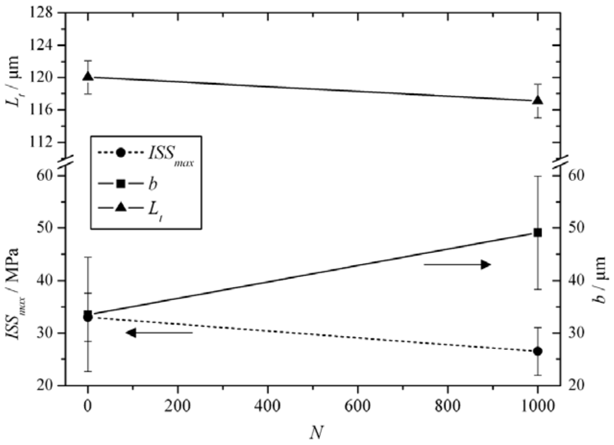

Fig. 10. Mean value of both fibre ends alongside the natural discontinuity, of the maximum interfacial shear stress, ISS_{max}, parameter b and of the stress transfer length, L_t, after 1 and 10^3 loading cycles (specimen "iftg-01").

value of 1.4 GPa at a distance of 150 μm from the tip. After 10^3 cycles, the starting value has not changed, and the maximum value of 1.7 GPa is attained at the same distance of 150 μm from the fibre end. The first alteration in the shape of the axial stress profiles is noted after 10^4 loading cycles where stresses appear to relax at the vicinity of the discontinuity. On the other hand, the maximum stress values and the corresponding transfer lengths remain unchanged. After 10^5 loading cycles, stress starts to build from zero and attains a maximum value of 1.6 GPa within 150 μm from the fibre end.

The effect of fatigue on the interface is investigated again by means of the change in the interfacial parameters as a function of loading cycles. ISS_{max}, b and L_t after 1, 10^3, 10^4 and 10^5 loading cycles, were calculated by application of Eq. (1) to the regressions on the axial stress distributions in Fig. 11 and are presented in Fig. 12. The maximum interfacial shear stress, ISS_{max}, decreases from 58 MPa after the first cycle, to 25 MPa after 10^4 cycles, and remains unchanged up to 10^5 cycles. The length required for the attainment of the ISS_{max}, b, increases gradually with loading cycles to a range of 45–55 μm after 10^4 cycles. The stress transfer length, L_t, appears to increase from 160 μm after the first cycle to 190 μm after 10^3 loading cycles, and remains practically constant thereafter.

The above experimental findings provide for the first time direct evidence at the microscale of the deleterious effect of fatigue loading upon interface performance. It is important to state that the changes of the interfacial parameters emanate purely from fatigue loading and are at no extent associated with the prolonged residence times, of the order of 48 h, at high loads. This is because, as shown earlier, the axial stresses in the fibres do not change significantly, even after 1000 h of residence at such load levels [12].

3.2.2. At "random" locations

Additional Raman measurements were performed during each interruption at "random" locations defined as knots of an imaginable 20 × 10 matrix grid on the surface of specimens "iftg-01" and "iftg-02" (Fig. 4). The experimental protocol allowed the movement of the Raman probe to the nearest neighbouring fibre in the case where the location of the imaginable knot did not coincide with a visible fibre. Fig. 13 depicts the mean values and associated standard deviations of 200 axial stress measurements performed on visible fibres, at each loading step, for the two specimens.

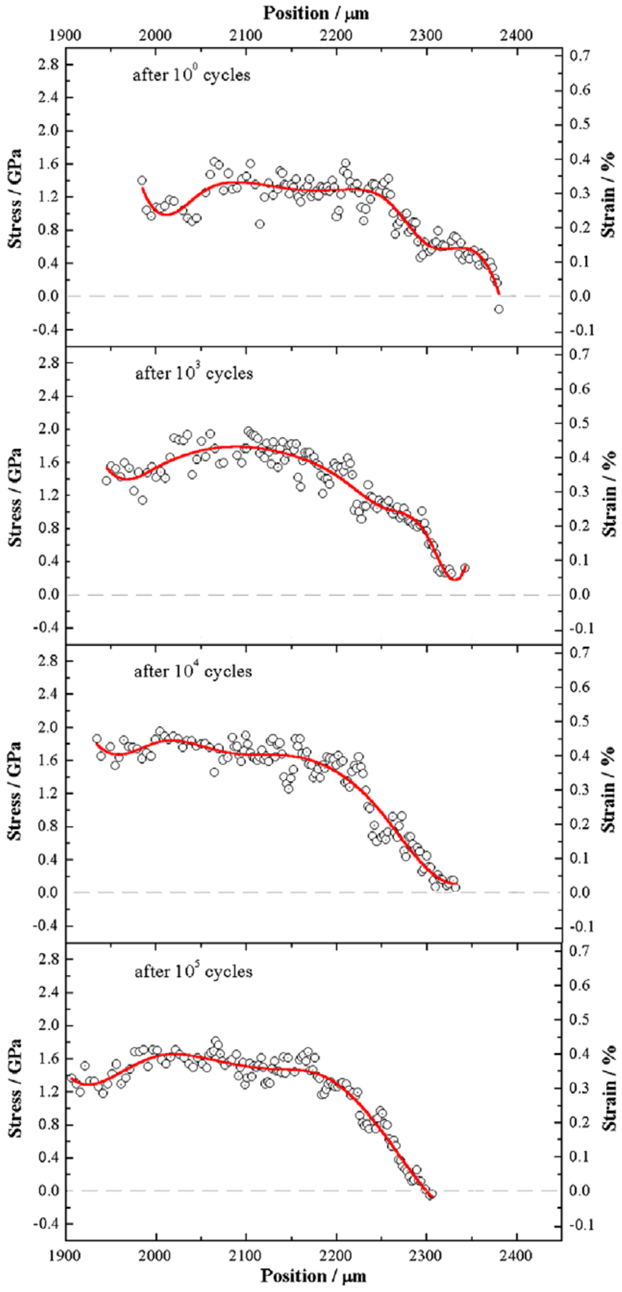

Fig. 11. Axial stressprofiles alongside a natural discontinuity after 1, 10^3,10^4 and 10^5 loading cycles (specimen "iftg-02").

The mean axial stress shown at zero cycles in both figures corresponds to the residual compressive stresses as a result of the laminate autoclave processing. These values, as well as the corresponding standard deviations, are iden-

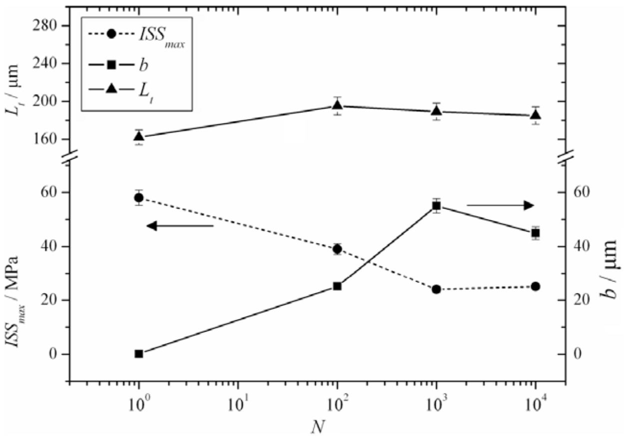

Fig. 12. Effect of loading cycles, N, on the maximum interfacial shear stress, ISS_{max}, on the distance b, from the discontinuity, required for the attainment of ISS_{max}, and on the transfer length, L_t (specimen “iftg-02”).

tical for the two specimens taken from the same laminate and are the average of all 400 measurements under zero applied strain. The calculated mean value of residual stress of −0.2 GPa is the same as that calculated around the natural discontinuity in specimen “iftg-01” as well as in specimen “itns-07” that was tested in tension and that originated from another laminate. This observation provides additional confirmation that the residual fibre stress in the specific fibre/matrix system, cured under the standard polymerization cycle proposed by the matrix manufacturer, is equal to −0.2 GPa (−0.05%).

The mean of 200 axial stresses measured via the Raman technique for specimen “iftg-01” after the first loading cycle is 1.4 GPa (0.35% strain) while a marginal increase to 1.5 GPa (0.38% strain) is noted after 10^3 cycles, mainly due to the small variation in the externally applied load. For specimen “iftg-02”, the mean value of 200 Raman measurements of axial stresses on visible fibres remains within the range of 1.2–1.4 GPa throughout the experiment. These values are expected to be somehow lower compared to those measured in the previous case (specimen “iftg-01”) since specimen “iftg-02” was subjected to lower externally applied loads. The standard deviation of the measurements after 10^3 cycles is 0.38 GPa and appears to decrease with the number of cycles. This observation indicates that the cyclic loading procedure tends to homogenize the stress state within the composite due to microcrack growth parallel to the loading axis and to increase debond lengths [13].

4. Discussion

4.1. Natural vs. induced discontinuities

The interfacial performance parameters, ISS_{max}, b and L_t, were presented in Fig. 8 for specimen “itns-07” tested under interrupted tensile loading conditions. The divergence observed between the parameters’ values collected alongside induced and natural discontinuity cases can be the result of the method of introduction of the induced discontinuity. Thereby, it is probable that the use of the surgical scalpel caused a local bending of the fibre ends, an effect that did not revert during thermal curing, but only after a tensile field was applied to the material. The example of stress distribution profile on the right of the induced discontinuity (Fig. 5) is characteristic: Stresses at the vicinity of the discontinuity start of from a tensile value, an observation indicating that the fibre is slightly bent towards the inner part of the specimen. Additionally, the fact that parameter b (Fig. 8) starts from non-zero values at the first loading stages and decreases to zero throughout loading, indicates that even at high externally applied strains no interfacial failure has occurred; hence the initial non-zero values can be attributed to fibre curvature effects.

In interrupted fatigue loading under constant stress conditions, a comparison between the interfacial performance parameters of the two specimens tested in fatigue loading, “iftg-01” and “iftg-02”, demonstrates that the values of ISS_{max}, b and L_t, attained by the latter specimen, are higher. This behaviour does not signify a lower quality interface in specimen “iftg-01”; on the contrary, an interfacial failure in the first loading cycle is anticipated near the natural discontinuity on specimen “iftg-01” as an outcome of the fibre recoiling upon fracture and the dissipation of the locally released energy to the interface [10]. Moreover, the fragment length appears to be lower than the critical length required for reinforcement, therefore the maximum stress/strain in the middle of the fragment is lower than expected. None of these mechanisms acts around the individual fibre in specimen “iftg-02”, which provides a measure of the “far field” values of the interfacial properties. It is thereby understood that, in a full composite material, interfacial properties are greatly influenced by the fibre failure mechanism and that interfacial performance is expected to be lower than the predictions of laboratory single-fibre coupons. At this point, it is important to note that similar experimental quantification of the effect of fatigue on the interfacial performance of full composite materials has not been offered in the past.

4.2. Evaluation of “random” measurements

To evaluate the results of LRM measurements at “random” locations on specimens “iftg-01” and “iftg-02”, a statistical analysis of the skewness and kurtosis measures of the corresponding populations, appears interesting. In brief, a set of values has a null skewness when their distribution is symmetric around the mean, while a positive or negative skewness signifies accumulation of data in values that are lower or higher than the mean, respectively. Similarly, a set of values of null kurtosis distributes normally around the mean, while positive or negative kurtosis measures indicate distributions that are wider or narrower than the normal distribution, respectively.

The skewness and kurtosis measures of the sets of 200 measurements as a function of the number of loading cycles are depicted in Figs. 14 and 15 for specimens “iftg-01” and “iftg-02”. The residual values, which are common for both specimens, appear to be associated with negative skewness and kurtosis measures; an observation that signifies an asymmetric, wider than the normal, distribution around the mean with data accumulating towards higher compressive values, probably as a result of stress concentration phenomena.

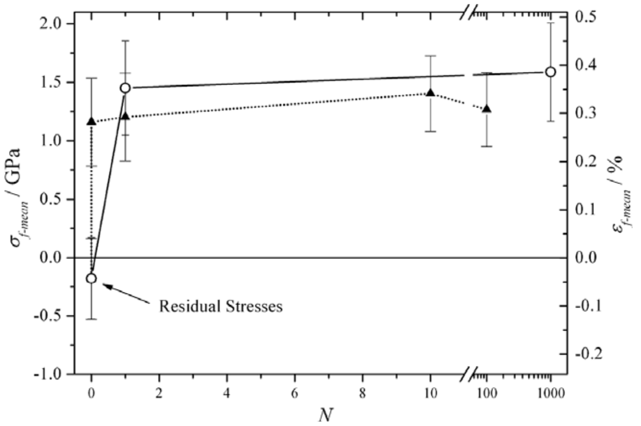

Fig. 13. The mean value and standard deviation (error bars) of 200 measurements of axial stress on equal in number surface fibres on specimens “iftg-01” and “iftg-02” as a function of loading cycles, *N*.

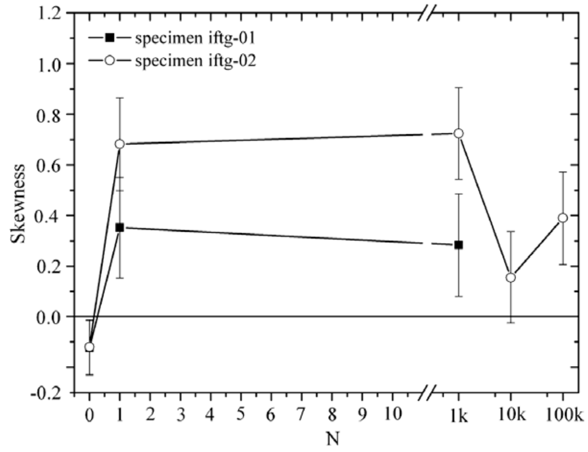

Fig. 14. Evolution of the skewness measure of the axial stress distributions as a function of loading cycle, for specimens “iftg-01” and “iftg-02”.

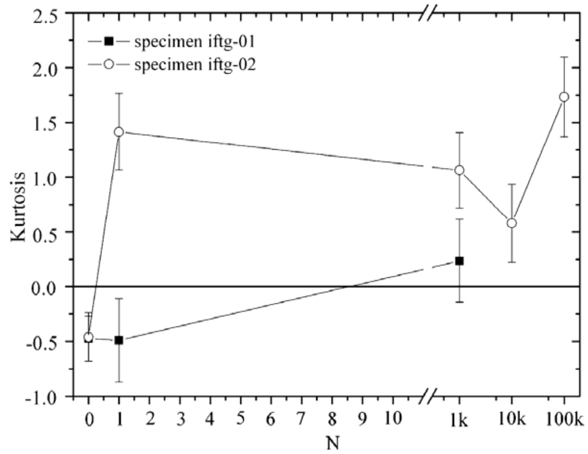

Fig. 15. Evolution of the kurtosis measure of the axial stress distributions as a function of loading cycle, for specimens “iftg-01” and “iftg-02”.

The skewness values for specimen “iftg-01” (Fig. 15) demonstrate that the asymmetry in the distribution of axial stresses changes sign after the first loading cycle to values higher that the instant mean tensile stress, while the width of the distribution remains unchanged. After 10^3 loading cycles, the skewness measure remains unchanged at positive signs while the kurtosis measure changes sign to positive values, indicating that the axial stresses at that cycle are more concentrated around the mean.

The change in skewness within the two first steps of measurements on specimen “iftg-02”, at 0 and 1 cycles, appears to be similar with the previous case. The fact that the overall skewness values are twice those of specimen “iftg-01” signifies that a greater number of axial stresses were collected from stress concentration areas. The asymmetry measure remains constant throughout the first and 1000th cycle, while it decreases after 10^4 cycles and increases again till the failure of the specimen.

It is argued that during the first loading cycles, loading contributes to the levelling of the stress field through microcrack growth and increase in debond length, while after 10^4 cycles, and up to specimen failure, stress concentration increases due to the gradual failure of an increasing number of fibres; hence the effect of fatigue becomes more apparent. The same levelling in axial stresses distribution up to 10^4 cycles is noted by observation of the kurtosis measure, while axial stresses appear to concentrate again around the mean at that number of cycles, just before the failure of the specimen (Fig. 15). The combination of values of the two measures shows that, at 10^5 cycles, the distribution of axial stresses on the fibres was intensely concentrated around the mean (that remain constant throughout testing, Fig. 13) while an additional accumulation at high stress concentration values was also noted. The evolution in the values of the two measures shows that, while stresses were initially concentrated at various locations, these areas disappear gradually with cyclic loading as the interfacial failure/debonding mechanism redistributes the stresses to a higher volume of fibres [13]. The latter mechanism ceases to dominate the mechanical behaviour of the material after a certain number of cycles, when fibre failure becomes the dominant damage mechanism, to allow the development of more stress concentration sites up to catastrophic failure. The above result is another indication of the negative effect of fatigue loading upon the fibre strength distribution and, ultimately, on the mechanical performance of the material.

5. Conclusions

The micromechanics of tension–tension fatigue loading in unidirectional C_f/epoxy coupons processed via the autoclave route are quantified directly at the microscale and in real time with the help of the LRM technique. Using the LRM method, the residual stresses on the fibres for the specific composite and cure cycle, was found to be compressive at -0.2 GPa, or -0.05% strain. The axial stress distributions established at each strain level were used to obtain the ISS profiles and to calculate the three most important indicators of interface performance, namely the maximum interfacial shear stress, the length required for its attainment, and the transfer length of the interface, for the composite under investigation. The evolution of these three parameters as a function of loading cycles showed unequivocally the deteriorating effect of fatigue loading on the stress transfer efficiency of the interface. The statistical analysis, by means of the skewness and kurtosis measures, of additional 200 measurements of axial stresses on equally numbered locations on the surfaces of the specimens, demonstrated that microcrack growth and interfacial debonding are the primary damage mechanisms during the initial fatigue stages. Fibre failure and the resulting stress concentration in the embedded fibres is the mechanism controlling the ultimate life of the composite. Thereby, the fatigue life of the composite is dictated by the interaction and interdependence of three major damage parameters: fibre strength, the rate of evolution of interfacial damage and the rate of development of stress concentration in the embedded fibres.

Acknowledgements

The authors wish to thank the European Social Fund (ESF), Operational Program for Educational and Vocational Training II (EPEAEK II), and particularly the Program PYTHAGORAS for funding this work.

References

[1] Gao YC, Zhou LM. Theor Appl Fract Mech 1998;30:235–41.
[2] Nayfeh AH, Abdelrahman WG. Composites B 1999;30:233–43.
[3] Gamstedt EK, Sjögren BA. Compos Sci Technol 1999;59:167–78.
[4] Horst JJ, Salienko NV, Spoormaker JL. Composites A 1998;29:525–31.
[5] Galiotis C. In: Summerscales J, editor. Microstructural characterization of fibre-reinforced composites. Cambridge: Woodhead Publishers; 1998.
[6] Koimtzoglou C, Kostopoulos V, Galiotis C. Appl Phys A 2002;76:231–9.
[7] Parthenios J, Katerelos DG, Psarras GC, Galiotis C. Eng Fract Mech 2002;69:1067–87.
[8] Koimtzoglou C, Kostopoulos V, Galiotis C. Composites A 2001;32:457–71.
[9] Koimtzoglou C, Kostopoulos V, Galiotis C. Appl Phys A 2003;76:231–9.
[10] Paipetis A, Galiotis C. Composites A 1996;27:755–67.
[11] Kim J-K, Mai Y-M. Engineered interfaces in “fiber reinforced composites”. Amsterdam: Elsevier; 1998.
[12] Miyake T, Yamakawa T, Ohno N. J Mater Sci 1998;33:5177–83.
[13] Gamstedt EK. J Appl Polym Sci 2000;76:457–74.